Journal of Applied Electrochemistry (2021) 51:1241–1252
https://doi.org/10.1007/s10800-021-01573-x

RESEARCH ARTICLE

Theoretical analysis of transient solution phase concentration field in a porous composite electrode with time-dependent flux boundary condition

Long Zhou[1] · **Mohammad Parhizi**[2] · **Ankur Jain**[2]

Received: 18 January 2021 / Accepted: 22 April 2021 / Published online: 11 May 2021
© The Author(s), under exclusive licence to Springer Nature B.V. 2021

Abstract

Energy conversion and storage in a Li-ion cell involves multiple closely coupled transport processes, such as species diffusion through solid and solution phases in the electrode. Mathematical modeling of these processes is critical for fully understanding and optimizing the performance of a Li-ion cell. While a number of analytical and numerical models have been presented for solution phase diffusion, most of such work is based on the assumption of a constant current density. This paper presents analytical modeling of solution phase diffusion in a separate–electrode composite for a generalized, time-dependent current density. An analytical solution for the concentration field in a separator–electrode composite in such conditions is derived using the method of eigenfunction expansion. Good agreement with past work as well as numerical simulations is shown. Results for linear, periodic and step-function boundary conditions are discussed. The theoretical analysis presented here may help accurately model realistic processes where the applied current changes over time, for example, cyclic charge and discharge in an electric vehicle, or sudden changes in the battery load. Results presented here contribute towards the fundamental understanding of solution phase diffusion in Li-ion cells, and provide a basis for improving electrochemical energy conversion and storage processes.

Graphic abstract

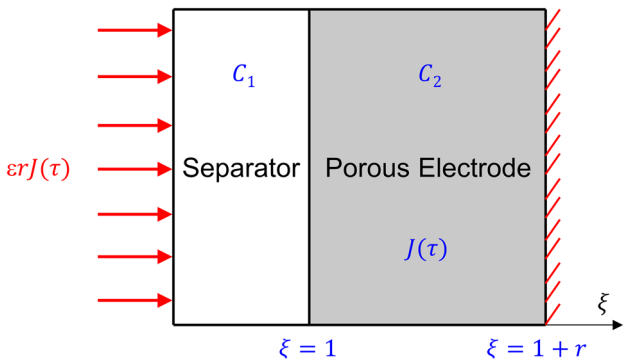

Keywords Li-ion cell · Solution phase diffusion · Species concentration · Analytical modeling

✉ Ankur Jain
jaina@uta.edu

[1] School of Mechanical and Power Engineering, Henan Polytechnic University, Jiaozuo, Henan, China

[2] Mechanical and Aerospace Engineering Department, University of Texas at Arlington, Arlington, TX, USA

Nomenclature

c	Concentration (mol m^{-3})
C	Non-dimensional concentration, $C = \frac{c}{c_0}$
c_0	Initial concentration (mol m^{-3})
D	Diffusivity (m^2 s^{-1})
F	Faraday constant (C mol^{-1})
I	Current density (A/m^2)

J Non-dimensional generation/consumption term, $J = -\frac{I(1-t^+)L_1^2}{FDL_2c_0\varepsilon}$
L Layer thickness (m)
r Ratio of electrode and separator thicknesses, $r = \frac{L_2}{L_1}$
t_+ Transference number (s)
t Time (s)
x Spatial coordinate (m)
ε Porosity
λ Eigenvalue
τ Non-dimensional time, $\tau = \frac{Dt}{L_1^2}$
ξ Non-dimensional spatial coordinate, $\xi = \frac{x}{L_1}$

Subscripts

1 Separator
2 Electrode

1 Introduction

Li-ion cells offer excellent electrochemical performance for energy storage and conversion in multiple applications such as consumer electronics, power grid, electric vehicles, military and space applications [1–4]. The operating mechanism of Li-ion batteries involves multiple transport phenomena triggered by different forcing functions. These processes are multiscale in nature, and are often coupled with each other [5, 6]. Modeling and optimizing these processes is critical to achieve favorable performance and efficiency for electrochemical systems [7, 8]. Significant research has been reported for developing battery models for various operating conditions. These include equivalent circuit models [9], empirical equations [10] and electrochemical models [11].

Empirical or data-based models use past experimental data for real-time estimation of Li-ion batteries states [12]. Although empirical models are often simple and computationally fast, they do not provide insights into the physical processes occurring in Li-ion cells and their related parameters [8, 11]. Equivalent circuit-based models are simplified mathematical models which use equivalent resistive and capacitive components to predict the behavior of Li-ion batteries [13, 14]. Similar to empirical models, circuit-based models do not provide details on the electrochemical processes inside Li-ion batteries.

In contrast, electrochemical or physics-based models predict the behavior of Li-ion cells by solving the differential equations that govern electrochemical reactions, mass, charge and thermal transport processes occurring in the cell [15]. These models often result in highly coupled partial differential equations for electrolyte, electrodes and separator [16]. Early work in the modeling of Li-ion batteries started with porous electrode theory presented by Newman and Tiedemann [17]. Later, using this porous electrode theory in combination with concentrated solution theory, Doyle, et al. presented Pseudo-2D model (P2D) [18], which has been used extensively. P2D model involves solving for the concentration of Li^+ ions in solid and liquid phases in conjunction with the solid and liquid phase potentials, and the Butler–Volmer equation [19]. This usually results in coupled, non-linear equations, for which, full analytical solutions are difficult to obtain [20]. Therefore, a variety of numerical and approximate analytical solutions have been developed to solve P2D model [21–26]. Numerical solutions are often computationally expensive due to the large number of equations [27] and a number of studies have been reported to reduce the computational time [27–29]. If the concentration gradient and potential in the solution phase is negligible, for example at low C-rates and for thin electrodes, the solid phase diffusion is the dominant process, and the P2D model can be reduced to the much simpler Single Particle Model [30, 31]. SPM only involves solving the solid-state concentration and Butler–Volmer equation, which is much simpler and faster solution than the P2D model [30, 31].

In contrast with numerical solutions, there is a relative lack of exact analytical solutions for transport problems in a Li-ion cell. Early work in this direction was presented by Doyle and Newman [32] for a few limiting cases, namely solid phase diffusion limitation, solution phase diffusion limitation and ohmically dominated cell. In the solid phase diffusion limitation case, the concentration gradient in the electrolyte can be neglected. This may occur when the applied current is low to moderate or when the electrodes are thin enough. In the solution phase diffusion limitation, the kinetic and solid phase diffusion are neglected and concentration gradient in the electrolyte becomes dominant. Finally, kinetic, solid and solution phase diffusion limitations are neglected in the Ohmically dominated cell. Fick's law of diffusion and concentrated solution theory were used to define the governing equations for solid phase diffusion limitation and solution phase diffusion limitation, respectively [32]. An average value for pore wall flux was used, which eliminated the need for solving Butler–Volmer equation, and resulted in uncoupled differential equations [32]. Separation of Variable technique was then used to solve for the concentration profiles in solid and solution phases [32].

The separation of variables (SOV) technique has also been used to solve for the solid phase diffusion limitation in other scenarios, such as a thin film electrode, spherical electrode particle and composite electrodes under constant current condition [33]. A solution for the solution phase diffusion limitation for a separator-porous electrode Li-ion cell has been also presented [33]. Short-time solution for Li-ion concentration has been derived using Laplace Transformation technique [34]. This method has been extended to derive both short-term and long-term solutions for solid and solution phase diffusion limitation

under galvanostatic boundary condition and non-zero initial condition [35]. Integral transform method has been used to address problems with constant [36] and time-dependent [37] flux boundary conditions. An analytical solution for solution phase diffusion limitation under galvanostatic boundary condition has been presented using Green's function method [38].

Most of the literature summarized above assumed a constant boundary condition that does not change with time. In practical scenarios, however, the applied current density may change significantly over time in response to changes in external conditions. For example, this could occur in the operation of an electric vehicle, where the electrical load may change with time. In addition, during cyclic charge/discharge of cells, the sign of the applied current density may completely reverse over time. Analytical models that accounts for such time-dependent boundary conditions are clearly desirable for modeling practical scenarios, but are rather uncommon in the literature. For example, an exact solution for solid phase diffusion under time-dependent flux boundary conditions for different cathode geometries using Green's function approach has been presented [39]. An analytical solution for liquid phase diffusion in a spherical electrode with time-dependent boundary conditions has been presented [37]. In addition, approximate solutions have been developed for time-dependent boundary conditions [40].

This paper presents an analytical solution for Li-ion diffusion in the solution phase of a composite porous electrode operating under time-dependent flux boundary condition, time-dependent reaction rate and arbitrary initial conditions using a multilayer SOV approach. While the reaction rate distribution in general is a function of both location and time, $J(x,t)$, it has been shown [32] that spatial distribution can be neglected in the solution phase diffusion limitation. The present work generalizes past models based on constant current by considering a time-dependent applied current and consequently a time-dependent reaction rate. The solution for concentration in each layer is derived in the form of an infinite series with well-defined coefficients and eigenvalues. Verification of the SOV technique by comparison against previous studies and numerical simulations is presented. Concentration profiles are determined for a variety of realistic charge/discharge conditions. The theoretical model presented here may be a useful mathematical tool for understanding and improving the performance of Li-ion cells and other related energy storage and conversion devices [41].

2 Analytical modeling

2.1 Governing equations

Consider Li ion diffusion in a cell comprising Lithium foil, separator and a porous positive electrode as shown in Fig. 1. The governing equations, initial and boundary conditions for

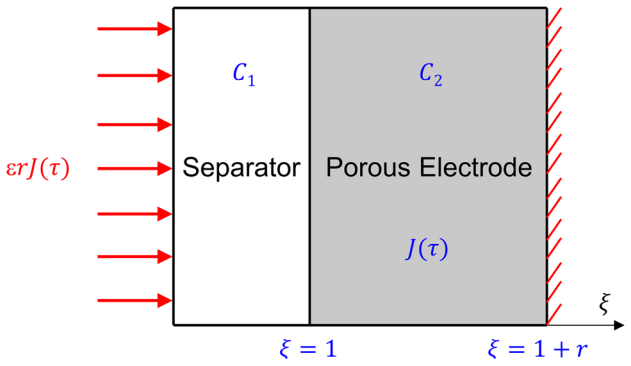

Fig. 1 Schematic of geometry for solution phase diffusion in a two-layer porous electrode

solution phase diffusion limitation have been originally presented by Doyle and Newman [32] and have been used widely in later studies [26, 33, 38]. Here, these equations are extended for time-dependent flux and reaction terms, as may occur during cyclic charge/discharge of the cell.

Similar to past work, the transference number t_+ is assumed to be constant, based on which, the migration term in the concentration conservation equation can be neglected. This is a reasonable assumption because ion mobilities in a Li-ion cell may be assumed to be independent of concentration [42]. A constant and uniform pore wall flux, given by $j_n = -\frac{I(1-t_+)}{F(L_2-L_1)}$ is assumed [32]. This assumption is valid if kinetic resistances dominate Ohmic resistances or if the cell's open-circuit potential strongly depends the state of charge of the system [26, 32]. Based on these assumptions, the dimensional set of equations and non-dimensional process are given in detail in Appendix A. Using the non-dimensional scheme presented in the Nomenclature section, the governing equations are given in dimensionless form by the following equations:

$$\frac{\partial C_1}{\partial \tau} = \frac{\partial^2 C_1}{\partial \xi^2}; \quad 0 < \xi < 1 \tag{1}$$

$$\frac{\partial C_2}{\partial \tau} = \varepsilon^{1/2} \frac{\partial^2 C_2}{\partial \xi^2}; \quad 1 < \xi < 1 + r \tag{2}$$

$$\frac{\partial C_1}{\partial \xi} = \varepsilon r J(\tau); \quad \xi = 0 \tag{3a}$$

$$\frac{\partial C_2}{\partial \xi} = 0; \quad \xi = 1 + r \tag{3b}$$

$$C_1 = C_2; \quad \xi = 1 \tag{3c}$$

$$\frac{\partial C_1}{\partial \xi} = \varepsilon^{3/2}\frac{\partial C_2}{\partial \xi}; \quad \xi = 1 \tag{3d}$$

$$C_1 = 1; \quad \tau = 0, \quad 0 < \xi < 1 \tag{4a}$$

$$C_2 = 1; \quad \tau = 0, \quad 1 < \xi < 1 + r \tag{4b}$$

where

$$J(\tau) = -I(\tau)\frac{\left(1 - t_+\right)L_1^2}{FDL_2c_0\varepsilon} \tag{5}$$

Equations (1)–(3), as well as all subsequent equations involving time-dependent variables are valid for $\tau > 0$. As listed in "Appendix A", the non-dimensional time and space coordinates, τ and ξ are defined as $\tau = \frac{Dt}{L_1^2}$ and $\xi = \frac{x}{L_1}$. In addition, $C_i = \frac{c_i}{c_0}$ and $r = \frac{L_2}{L_1}$, where c_1 and c_2 are the concentrations in the separator and porous electrode, respectively.

Note that Eqs. (1) and (2) govern the concentration of electrolyte in the separator and the solution phase of the porous electrode, respectively. Equation 3a describes the relationship between the discharge rate and the mass flux at the Li-foil while Eq. 3b ensures that no flux leaves from the back of the electrode that is connected to the current collector. Equations 3c and 3d ensure the continuity of the concentration and flux at the separator–electrode interface. Note that the present analysis assumes a time-varying current.

The next section presents an analytical method to derive a closed form solution of Eqs. (1)-(4).

2.2 Solution method

2.2.1 Homogenization of boundary conditions

In order to derive a solution for the species diffusion problem defined in the previous section, the concentration distribution $C_i(\xi,\tau)$ is first split into two parts [43]

$$C_i(\xi, \tau) = \phi_i(\xi, \tau) + g_i(\xi, \tau) \tag{6}$$

where $\phi_i(\xi,\tau)$ is the unsteady-state component of the solution that accounts for the internal source term and homogeneous boundary conditions, while $g_i(\xi,\tau)$ accounts for the non-homogeneous boundary condition.

The motivation to split the solution into two parts is to absorb the non-homoegeneous boundary condition, Eq. (3a) into g_i, so that the other part of the solution, $\phi_i(\xi,\tau)$, can be solved using the separation of variables method. Note that g_i does not need to satisfy the governing equations, as long as the governing equations for ϕ_i are written in such a way that the sum of g_i and ϕ_i satisfies the governing equations.

Therefore, the following expression is assumed for the second component $g_i(\xi,\tau)$

$$g_i(\xi, \tau) = R_i(\tau)\xi^2 + S_i(\tau)\xi \tag{7}$$

The functions $R_i(\tau)$ and $S_i(\tau)$ are determined by requiring $g_i(\xi,\tau)$ to satisfy boundary conditions similar to Eqs. (3a)–(3d), given by

$$\frac{\partial g_1}{\partial \xi} = \varepsilon r J(\tau); \quad \xi = 0 \tag{8a}$$

$$\frac{\partial g_2}{\partial \xi} = 0; \quad \xi = 1 + r \tag{8b}$$

$$g_1 = g_2; \quad \xi = 1 \tag{8c}$$

$$\frac{\partial g_1}{\partial \xi} = \varepsilon^{3/2}\frac{\partial g_2}{\partial \xi}; \quad \xi = 1 \tag{8d}$$

Note that the boundary condition in Eq. (8a) is chosen to absorb the non-homogeneous boundary condition. Substituting Eq. (7) into Eqs. (8a)–(8d), the following expressions may be obtained for $R_i(\tau)$ and $S_i(\tau)$.

$$R_1(\tau) = -\varepsilon r J(\tau)\left[1 + \frac{1 + 2r}{2\left(r\varepsilon^{3/2} - 1 - 2r\right)}\right] \tag{9a}$$

$$S_1(\tau) = \varepsilon r J(\tau) \tag{9b}$$

$$R_2(\tau) = \frac{\varepsilon r J(\tau)}{2\left(r\varepsilon^{3/2} - 1 - 2r\right)} \tag{9c}$$

$$S_2(\tau) = -\frac{(1 + r)\varepsilon r J(\tau)}{r\varepsilon^{3/2} - 1 - 2r} \tag{9d}$$

This results in determination of $g_i(\xi,\tau)$ according to Eq. (7). The remainder of the solution, $\phi_i(\xi,\tau)$ has homogeneous boundary conditions, and is solved next.

2.2.2 Solution of the component with homogeneous boundary conditions

A governing partial differential equation for $\phi_i(\xi,\tau)$ can be derived by substituting Eq. (6) into Eqs. (1) and (2) and using expression (7). Since $g_i(\xi,\tau)$ does not necessarily satisfy the governing differential equation or the initial condition, the following equations are derived for $\phi_i(\xi,\tau)$ in order to ensure that the sum of g_i and ϕ_i satisfies Eqs. (1) and (2):

$$\frac{\partial \phi_1}{\partial \tau} = \frac{\partial^2 \phi_1}{\partial \xi^2} + Q_1(\xi, \tau); \quad 0 < \xi < 1 \tag{10}$$

$$\frac{\partial \phi_2}{\partial \tau} = \varepsilon^{1/2} \frac{\partial^2 \phi_2}{\partial \xi^2} + Q_2(\xi, \tau); \quad 1 < \xi < 1 + r \tag{11}$$

where

$$Q_1(\xi, \tau) = 2R_1(\tau) - \dot{R}_1(\tau)\xi^2 - \dot{S}_1(\tau)\xi \tag{12a}$$

$$Q_2(\xi, \tau) = J(\tau) + 2\varepsilon^{1/2} R_2(\tau) - \dot{R}_2(\tau)\xi^2 - \dot{S}_2(\tau)\xi \tag{12b}$$

Note that the over-dot stands for the derivative with respect to τ.

The functions $\phi_i(\xi, \tau)$ are subject to the following boundary conditions

$$\frac{\partial \phi_1(0, \tau)}{\partial \xi} = 0 \tag{13a}$$

$$\frac{\partial \phi_2(1 + r, \tau)}{\partial \xi} = 0 \tag{13b}$$

$$\phi_1(1, \tau) = \phi_2(1, \tau) \tag{13c}$$

$$\frac{\partial \phi_1(1, \tau)}{\partial \xi} = \varepsilon^{3/2} \frac{\partial \phi_2(1, \tau)}{\partial \xi} \tag{13d}$$

Finally, by introducing Eqs. (6) into (4), the initial condition becomes

$$\phi_i(\xi, 0) = 1 - g_i(\xi, 0) \tag{14}$$

Equations (10)–(14) represent a pair of partial differential equations with homogeneous boundary conditions and non-homogeneous initial condition. Further note that each of the partial differential equations contains a non-homogeneous source term.

In order to solve these equations, series forms are assumed for $\phi_1(\xi, \tau)$ and $\phi_2(\xi, \tau)$ as follows:

$$\phi_1(\xi, \tau) = q_0(\tau) + \sum_{n=1}^{\infty} \psi_{1,n}(\xi) q_n(\tau); \quad 0 < \xi < 1 \tag{15}$$

$$\phi_2(\xi, \tau) = q_0(\tau) + \sum_{n=1}^{\infty} \psi_{2,n}(\xi) q_n(\tau); \quad 1 < \xi < 1 + r \tag{16}$$

where $\psi_{1,n}(\xi)$ and $\psi_{2,n}(\xi)$ are the eigenfunctions for the first and second layers separately, and $q_0(\tau)$ and $q_n(\tau)$ are the time-dependent variable functions.

By inserting the form of the solution in boundary conditions, the eigenfunctions are found to be

$$\psi_{1,n}(\xi) = \cos\left(\lambda_n \xi\right) \tag{17a}$$

$$\psi_{2,n}(\xi) = \eta_n \sin\left(\beta_n \xi\right) + \mu_n \cos\left(\beta_n \xi\right) \tag{17b}$$

where $\beta_n = \frac{1}{\varepsilon^{1/4}} \lambda_n$, $\eta_n = \frac{\cos(\lambda_n) \tan[\beta_n(1+r)]}{\tan[\beta_n(1+r)] \sin(\beta_n) + \cos(\beta_n)}$ and $\mu_n = \frac{\cos(\lambda_n)}{\tan[\beta_n(1+r)] \sin(\beta_n) + \cos(\beta_n)}$.

Using boundary conditions given by Eqs. (13a)–(13d), the eigenvalues λ_n can be shown to satisfy the following transcendental equation

$$\tan\left(\lambda_n\right) = -\varepsilon^{5/4} \tan\left(\beta_n r\right) \tag{18}$$

The orthogonality relationship is

$$\int_0^1 \psi_{1,m}(\xi)\psi_{1,n}(\xi)\mathrm{d}\xi + \varepsilon \int_1^{1+r} \psi_{2,m}(\xi)\psi_{2,n}(\xi)\mathrm{d}\xi = \begin{cases} 0 & m \neq n \\ N_n & m = n \end{cases} \tag{19}$$

where the norm is given by

$$N_n = \int_0^1 \psi_{1,n}^2(\xi)\mathrm{d}\xi + \varepsilon \int_1^{1+r} \psi_{2,n}^2(\xi)\mathrm{d}\xi \tag{20}$$

Introducing Eqs. (15) and (16) into Eqs. (10) and (11) results in

$$\dot{q}_0(\tau) + \sum_{n=1}^{\infty} \psi_{1,n}(\xi)\dot{q}_n(\tau) = \sum_{n=1}^{\infty} \psi_{1,n}''(\xi) q_n(\tau) + Q_1(\xi, \tau); \quad 0 < \xi < 1 \tag{21}$$

$$\dot{q}_0(\tau) + \sum_{n=1}^{\infty} \psi_{2,n}(\xi)\dot{q}_n(\tau) = \varepsilon^{1/2} \sum_{n=1}^{\infty} \psi_{2,n}''(\xi) q_n(\tau) + Q_2(\xi, \tau); \quad 1 < \xi < 1 + r \tag{22}$$

where $\psi''_{1,n}(\xi)$ and $\psi''_{2,n}(\xi)$ are the second-order derivatives of functions $\psi_{1,n}(\xi)$ and $\psi_{2,n}(\xi)$ with respect to ξ.

Expanding $Q_1(\xi,\tau)$ in Eq. (21) and $Q_2(\xi,\tau)$ in Eq. (22) in series form using $\psi_{1,n}(\xi)$ and $\psi_{2,n}(\xi)$ as the basis functions, Eqs. (21) and (22) may be recast as

$$\dot{q}_0(\tau)+\sum_{n=1}^{\infty}\psi_{1,n}(\xi)\dot{q}_n(\tau)=\sum_{n=1}^{\infty}\psi''_{1,n}(\xi)q_n(\tau)+\sum_{n=1}^{\infty}\psi_{1,n}(\xi)\gamma_n(\tau)+\gamma_0(\tau);\quad 0<\xi<1 \tag{23}$$

$$\dot{q}_0(\tau)+\sum_{n=1}^{\infty}\psi_{2,n}(\xi)\dot{q}_n(\tau)=\varepsilon^{1/2}\sum_{n=1}^{\infty}\psi''_{2,n}(\xi)q_n(\tau)+\sum_{n=1}^{\infty}\psi_{2,n}(\xi)\gamma_n(\tau)+\gamma_0(\tau);\quad 1<\xi<1+r \tag{24}$$

where

$$\gamma_0(\tau)=\frac{\int_0^1 Q_1(\xi,\tau)\mathrm{d}\xi+\varepsilon\int_1^{1+r}Q_2(\xi,\tau)\mathrm{d}\xi}{1+\varepsilon r} \tag{25}$$

$$\gamma_n(\tau)=\frac{\int_0^1 \psi_{1,n}(\xi)Q_1(\xi,\tau)\mathrm{d}\xi+\varepsilon\int_1^{1+r}\psi_{2,n}(\xi)Q_2(\xi,\tau)\mathrm{d}\xi}{N_n} \tag{26}$$

Note that $\gamma_0(\tau)$ and $\gamma_n(\tau)$ are known functions, since the functions $\psi_{i,n}(\xi)$ and $Q_i(\xi,\tau)$ are both known from Eqs. (17a)–(17b) and (12a)–(12b), respectively. Because $\dot{q}_0(\tau)$ and $q_n(\tau)$ are independent in Eqs. (23) and (24), for each n, one can let

$$\dot{q}_0(\tau)=\gamma_0(\tau) \tag{27}$$

$$\psi_{1,n}(\xi)\dot{q}_n(\tau)=\psi''_{1,n}(\xi)q_n(\tau)+\psi_{1,n}(\xi)\gamma_n(\tau);\quad 0<\xi<1 \tag{28}$$

$$\psi_{2,n}(\xi)\dot{q}_n(\tau)=\varepsilon^{1/2}\psi''_{2,n}(\xi)q_n(\tau)+\psi_{2,n}(\xi)\gamma_n(\tau);\quad 1<\xi<1+r \tag{29}$$

To obtain the initial condition $q_0(0)$, one can let the series sum in Eqs. (15) and (16) to be equal to zero and substitute Eq. (15) into Eq. (14), followed by integration with respect to ξ from $\xi=0$ to $\xi=1$. Also, Eq. (16) is multiplied with ε and integrated with respect to ξ from $\xi=1$ to $\xi=1+r$. The two resulting expressions are then added, which results in

$$q_0(0)=\frac{\int_0^1\left[1-g_1(\xi,0)\right]\mathrm{d}\xi+\varepsilon\int_1^{1+r}\left[1-g_2(\xi,0)\right]\mathrm{d}\xi}{1+\varepsilon r} \tag{30}$$

To obtain $q_n(\tau)$, Eq. (28) is multiplied by $\psi_{1,m}(\xi)$ and integrated with respect to ξ from $\xi=0$ to $\xi=1$. Equation (29) is multiplied by $\varepsilon\psi_{2,m}(\xi)$ and integrated with respect to ξ from $\xi=1$ to $\xi=1+r$. Finally, summing up the two resulting expressions and applying the orthogonality relationship (19) results in a much simplified ordinary differential equation for $q_n(\tau)$

$$\lambda_n^2 q_n(\tau)+\dot{q}_n(\tau)=\gamma_n(\tau) \tag{31}$$

In order to determine the initial condition for $q_n(\tau)$, Eqs. (15) and (16) are substituted in Eq. (14), which with the use of the orthogonality relationship given by Eq. (19), results in

$$q_n(0)=\frac{\int_0^1\psi_{1,n}(\xi)\left[1-g_1(\xi,0)\right]\mathrm{d}\xi+\varepsilon\int_1^{1+r}\psi_{2,n}(\xi)\left[1-g_2(\xi,0)\right]\mathrm{d}\xi}{N_n} \tag{32}$$

The ordinary differential equations for $q_0(\tau)$ and $q_n(\tau)$, given by Eqs. (27) and (31), and subject to initial conditions given by Eqs. (30) and (32) have straightforward solutions, given by

$$q_0(\tau)=q_0(0)+\int_0^{\tau}\gamma_0(\tau^*)\mathrm{d}\tau^* \tag{33}$$

$$q_n(\tau)=e^{-\lambda_n^2\tau}\left\{q_n(0)+\int_0^{\tau}\gamma_n(\tau^*)e^{\lambda_n^2\tau^*}\mathrm{d}\tau^*\right\} \tag{34}$$

This completes the solution. Substituting Eqs. (7), (15), (16), (17a) and (17b) into Eq. (6), the analytical solutions for the concentration distribution are given by

$$C_1(\xi,\tau)=q_0(\tau)+\sum_{n=1}^{\infty}\cos\left(\lambda_n\xi\right)q_n(\tau)+R_1(\tau)\xi^2+S_1(\tau)\xi;\quad 0<\xi<1 \tag{35}$$

$$C_2(\xi,\tau)=q_0(\tau)+\sum_{n=1}^{\infty}\left[\eta_n\sin\left(\beta_n\xi\right)+\mu_n\cos\left(\beta_n\xi\right)\right]q_n(\tau)+R_2(\tau)\xi^2+S_2(\tau)\xi;\quad 1<\xi<1+r \tag{36}$$

3 Results and discussion

3.1 Effect of number of eigenvalues

Similar to any infinite series solution, the solution presented in this paper must be truncated to a finite number of terms for computation. The larger the number of terms considered, the greater is the accuracy, but so is the computational cost. The importance of determining the minimum number of terms for reasonable accuracy has been recognized [32]. For the present model, Fig. 2 analyzes the effect of number of eigenvalues on the accuracy of the resulting concentration profile. Specifically, Fig. 2a and b plot concentration

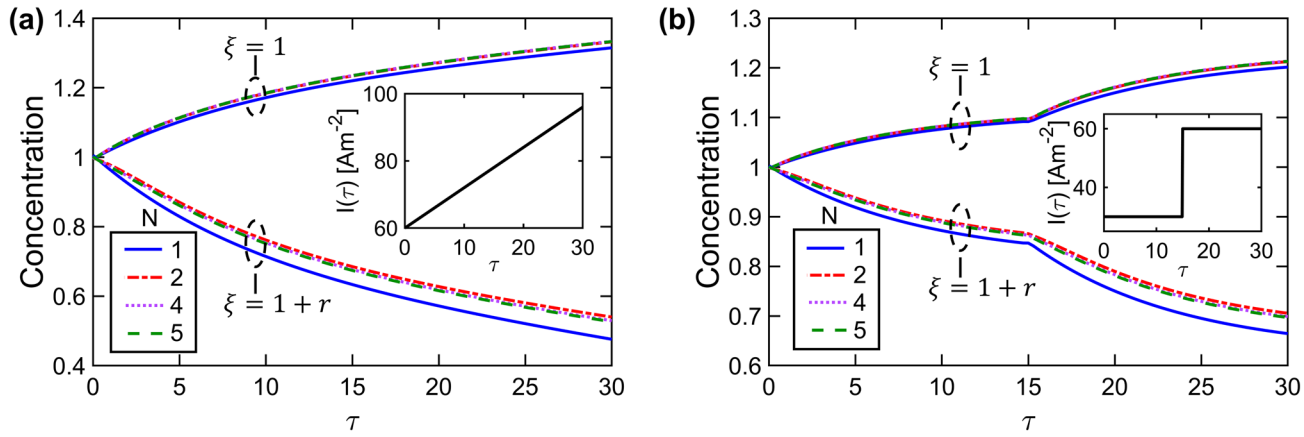

Fig. 2 Effect of number of eigenvalues: Concentration profile at $\xi = 1$ and $\xi = 1+r$ as functions of time for different number of eigenvalues, N, for two different current profiles: **a** Linear $I(\tau) = 60\left(1 + \frac{\tau}{50}\right)$ Am^{-2} and **b** Step function $I(\tau) = 30$ Am^{-2} for $0 < \tau < 15$ and $I(\tau) = 60$ Am^{-2} for $15 < \tau < 30$

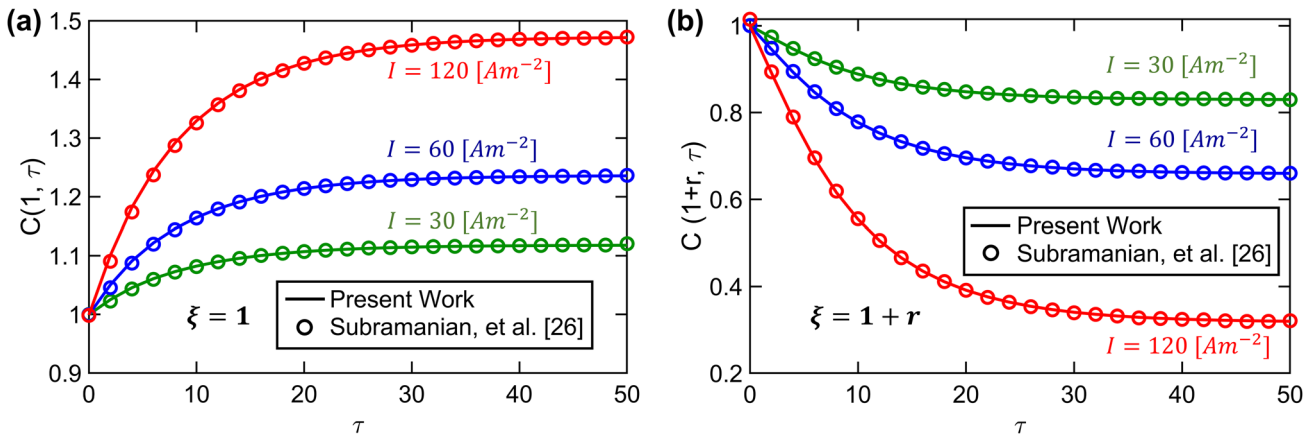

Fig. 3 Comparison of the analytical model with past work [26] for constant current density: **a** Concentration at the separator–electrode interface, $c_2(1, \tau)$, and **b** Concentration at the back of the electrode, $c_2(1 + r, \tau)$ as functions of τ for three different current densities. In each plot, curves represent the present analytical model, and symbols represent results by Subramanian, et al. [26]

profile as a function of time at $\xi = 1$ and $\xi = 1+r$ for 1, 2, 4 and 5 eigenvalues for a linearly increasing flux density and a step increase in the flux density, respectively. In both cases, the calculated distribution changes between the $N = 1$, $N = 2$ and $N = 4$ cases, but there is nearly no change between the $N = 4$ and $N = 5$ cases. This shows that around four to five eigenvalues are sufficient for accurate computation for the set of parameters considered in Fig. 2. All further plots in this paper are generated using five eigenvalues.

3.2 Model verification and comparison with past work

Since the analytical model in this paper generalizes past work on constant flux boundary condition, it is instructive to compare results based on the analytical model with these papers for the special case of constant current. Based on values of parameters such as diffusivity and porosity assumed by Subramanian et al. [26], Fig. 3a and b plot concentration at the separator–electrode interface and at the back of the electrode, respectively as functions of time for three different, constant current densities. The scenario considered in this plot is that of a porous cathode during a discharge process. In both plots, the analytical model presented in this work is compared with results from Subramanian et al. [26], for three different values of current density. Both Figures show excellent agreement between the two approaches, showing that the present work reduces to a well-established model for the special case of constant flux. While the concentration at the separator–electrode interface rises with

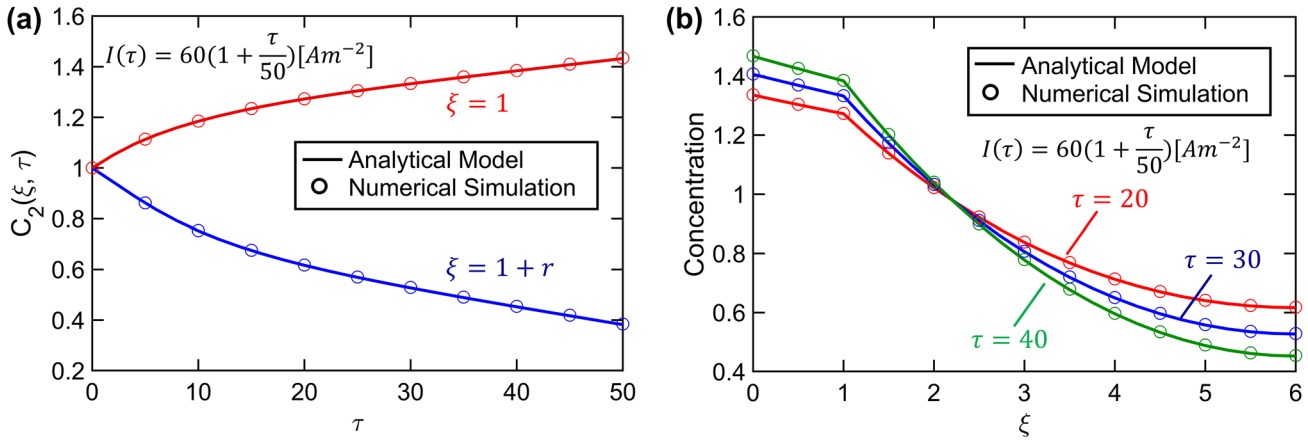

Fig. 4 Validation of the analytical model through comparison with numerical simulations: **a** Concentrations at the two ends of the electrode as functions of time; **b** Concentration distribution in the separator and electrode at three different times. In each case, $I(\tau) = 60\left(1 + \frac{\tau}{50}\right)\text{Am}^{-2}$. Comparison between analytical model and numerical simulations is presented in each plot

time due to species influx from the left, concentration at the end of the electrode reduces with time due to species consumption in the intercalation process. The greater the current density, the greater is the rate of rise and fall in concentrations at the two locations, respectively. Note that, while the past studies present solution for galvanostatic (constant current) discharge condition, the solution presented here is applicable to any arbitrary time-dependent current profile and it reduces to the result from past studies for the special case of constant current.

To further validate the analytical model for more general, time-dependent boundary conditions, results are compared against predictions from a numerical simulation for a linearly time-dependent boundary condition. A finite-difference based numerical simulation code is utilized for comparison. Note that the numerical simulation is also developed for the case of solution phase diffusion limitation. Thus, the same governing equations and boundary conditions (Eqs. (1)–(4)) solved analytically in Sect. 2 are discretized and solved numerically using a fully implicit approach. Each layer is discretized into 1000 nodes. Boundary conditions are applied at the two ends and continuity of concentration and flux at the interface of the two layers are applied to the node at the interface. Figure 4a presents comparison of concentration as a function of time at two different points in the electrode between the analytical model and numerical simulation for a current density of $I(\tau) = 60(1 + \tau/50)\ \text{Am}^{-2}$. In both cases, there is excellent agreement between the two. Further, Fig. 4b plots the entire concentration distribution

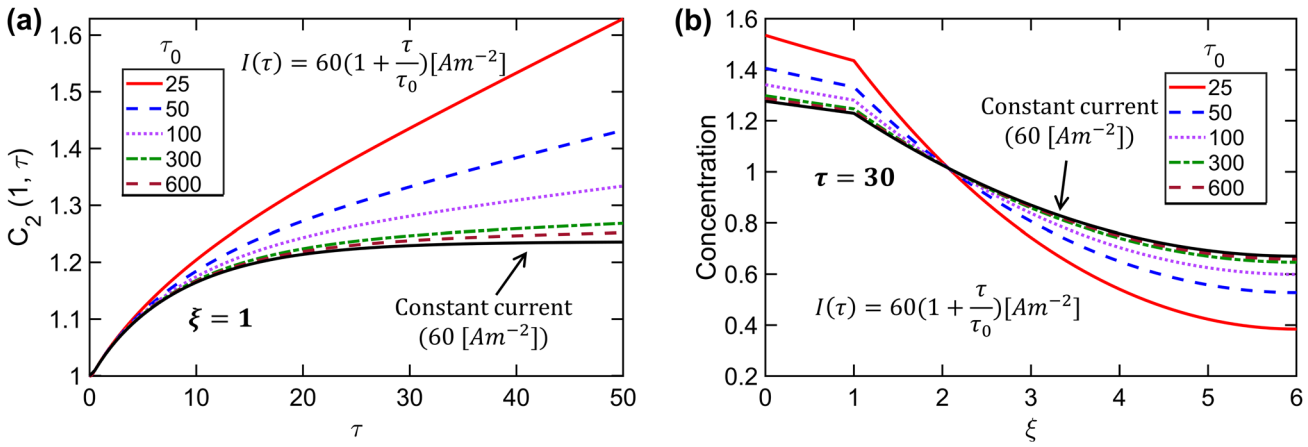

Fig. 5 Concentration profiles for linear flux density $I(\tau) = 60\left(1 + \frac{\tau}{\tau_0}\right)\text{Am}^{-2}$: **a** Concentration at the separator–electrode interface as a function of time; **b** Concentration distribution in the separator and electrode at $\tau = 30$. Curves are plotted for multiple values of τ_0. For reference, curves for the constant current density $I(\tau) = 60\text{Am}^{-2}$ are also plotted

in the separator and electrode at multiple times for the same current density. There is excellent agreement between the analytical model and numerical simulations over the entire domain at each time. These results provide additional confidence in the analytical model presented in Sect. 2.

In subsequent sub-sections, concentration distributions due to a variety of time-dependent current profiles are computed and presented.

3.3 Concentration profiles for linear concentration flux

Figure 5 plots the concentration field for linearly varying flux, $I(\tau) = 60\left(1 + \frac{\tau}{\tau_0}\right)\,\mathrm{Am}^{-2}$ for five different values of τ_0. In addition, curves corresponding to the constant current $I(\tau) = 60\,\mathrm{Am}^{-2}$ case are also shown. While Fig. 5a plots concentration at the separator–electrode interface as a function of time, Fig. 5b plots the spatial distribution of concentration at $\tau = 30$. Figure 5a shows that concentration at the separator–electrode interface rises much faster for the linear flux cases than the corresponding constant flux case. This is because there is greater species flux in the linear cases—the lower the value of τ_0, the greater is the overall species flux, and thus, the larger is the increase in concentration at the separator–electrode interface. This trend is also seen in Fig. 5b which shows that there is greater rise in concentration in the separator and greater reduction in concentration in the electrode as the value of τ_0 reduces. In both Figures, the concentration curve computed using the analytical model approaches the constant current case as the value of τ_0 becomes very large, as expected.

3.4 Concentration profiles for periodic concentration flux

Figure 6 analyzes the case where the current flux is a sinusoidal function of time. For two different frequencies, Fig. 6a plots concentrations at the separator–electrode interface and at the end of the electrode as functions of time. The periodic variation in the computed concentration profiles is clear from Fig. 6a, and the periodicity matches with the frequency of the imposed current. Figure 6b plots the concentration distribution in the separator and electrode as three different times for a sinusoidally varying current with $\omega = 1/20$. It is seen that concentration at the separator/electrode interface is largest at $\tau = 35$, followed by $\tau = 40$, and then $\tau = 20$. This is consistent with Fig. 6a where concentration is at its minimum and maximum at $\tau = 20$ and 35, respectively. Furthermore, the two curves at $\tau = 20$ and 40 are very close to each other due to the close values of their concentration seen in Fig. 6a. In contrast, the back of the electrode exhibits the opposite behavior—concentration is largest at $\tau = 20$, followed by $\tau = 40$, and then $\tau = 35$. This is also consistent with Fig. 6a. These Figures show that the present model can predict the periodic and non-monotonic behavior of the concentration profile both as a function of time and throughout the composite electrode at any given time.

3.5 Concentration profiles for step-function concentration flux

Step-function changes in the current density may also be of interest for practical applications. This is analyzed in the next two Figures.

Figure 7 considers a scenario where the current density undergoes two step changes. The current starts at 25 Am^{-2}, then increases to 45 Am^{-2} at $\tau = 10$, and to 60 Am^{-2}

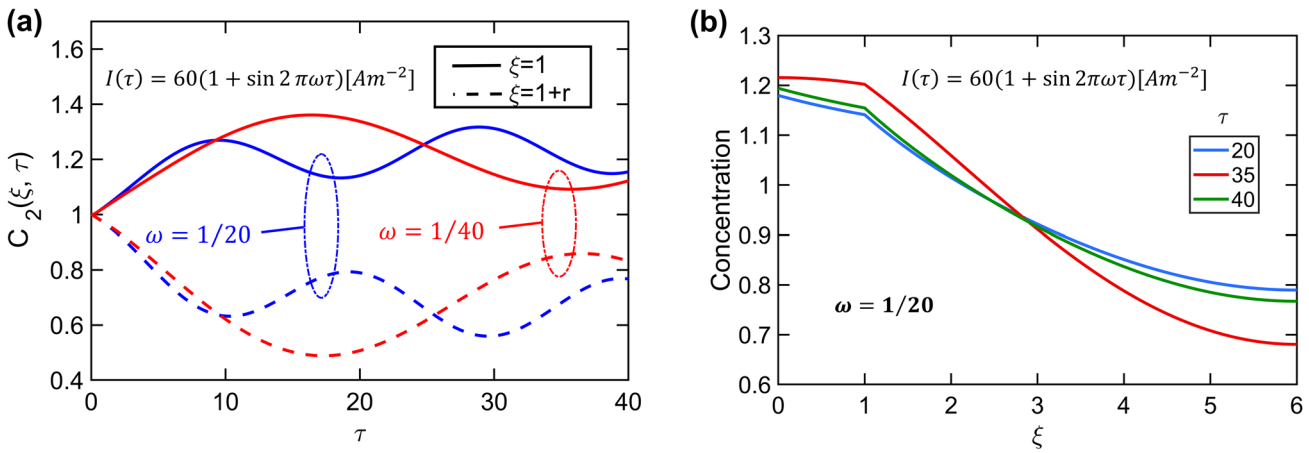

Fig. 6 Concentration profiles for sinusoidal current density $I(\tau) = 60[1 + \sin(2\pi\omega\tau)]\mathrm{Am}^{-2}$: **a** Concentrations at the two ends of the electrode as a function of time for two different values of ω; **b** Concentration distribution in the separator and electrode at three different times for $\omega = 1/20$

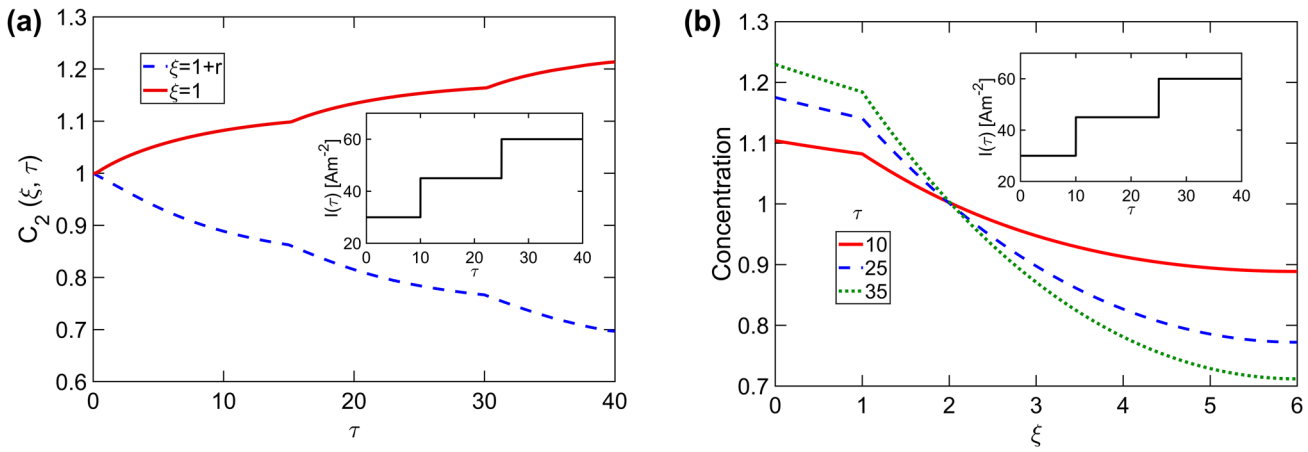

Fig. 7 Concentration profiles for step-function variation in current density, where the current density increases in two steps: **a** Concentrations at the two ends of the electrode as a function of time; **b** Concentration distribution in the separator and electrode at three different times. The inset shows step-variation in current density over time

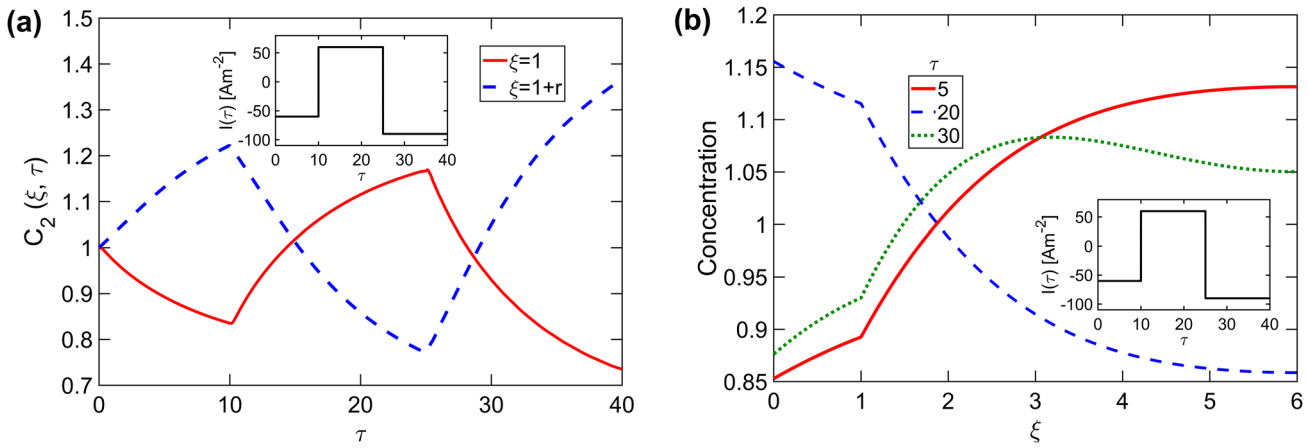

Fig. 8 Concentration profiles for step-function variation in current density, where the cell switches from charge to discharge, and then back to charge: **a** Concentrations at the two ends of the electrode as a function of time; **b** Concentration distribution in the separator and electrode at three different times. The inset shows step-variation in current density over time

at $\tau = 25$. Concentrations at the separator–electrode interface and at the end of the electrode are plotted as functions of time in Fig. 7a. There is a change in the slopes of the curves at each time corresponding to a step change. This is expected because, in this case, the current goes up at each step, and therefore, the rates of change of concentrations at the two locations must increase across the times of the step change. Figure 7b plots concentration distribution in the separator and electrode at three different times, two of which correspond to the step changes. As the current increases, concentration in the separator goes up due to added inwards flux, and concentration in the electrode towards the back goes down due to additional consumption. Concentration in the region in the electrode close to the separator rises due to greater influence of the inward flux. Such curves can be used to understand how the concentration distribution in the composite separator–electrode body changes when subjected to step changes in the current density.

Figure 8 considers a somewhat more complicated step-change scenario, where the cell charges for some time, then switches to discharge, and finally returns to charge. The concentration fields computed by the analytical model in Sect. 2 accurately account for these sudden changes. For example, Fig. 8a plots concentrations at the separator–electrode interface and at the end of the electrode as functions of time. Figure 8a clearly shows a change in direction of the concentration curves whenever the cell switches from charge to discharge, and vice versa. Concentration at the separator–electrode interface reduces initially while the cell is charging due to species outflux during charge. During the

discharge phase, concentration at the separator–electrode interface begins to rise because of flux into the separator during discharge. Finally, when the cell switches back to charge, the concentration begins to drop off again. The rate of reduction in the third phase is larger than in the first phase because of the larger charge current in the third phase. Figure 8b plots the spatial concentration distribution at three different times. At $\tau = 5$, while the cell is in charge phase, concentration has a positive slope, which is consistent with the outflux of species during charging process. During the discharge period, species influx occurs into the separator, which is why, the concentration field in the separator increases and the slope becomes negative during the discharge period. In each case, the concentration distribution in the electrode region is governed by the interplay between species influx/outflux and consumption/generation during periods of discharge and charge, respectively.

4 Conclusions

It is important to account for sudden or gradual changes in current density that may occur in realistic energy conversion and storage processes in a Li-ion cell. While most previous studies presented analytical solutions for concentration profile under galvanostatic discharge operating conditions, the novelty of this work is to extend previous studies and present a generalized solution applicable for any arbitrary, time-dependent current. While the analytical model presented in this work is more complicated than past work on constant current density, the final results are not overly complicated to compute. For example, the use of only a few eigenvalues has been shown to result in reasonable accuracy. The good agreement between the analytical model and past work for the special case of constant current density, as well as with numerical simulation results increases confidence in the analytical model. The results discussed for step-function changes in current density are directly relevant for applications where the current density may suddenly change magnitude and sign as the cell charges and discharges. Similarly, the analysis related to periodic functions may be helpful for analyzing applications where the current density as a function of time can be represented by a series comprising periodic functions. It is expected that the analytical model and its applications discussed here will improve the theoretical understanding of diffusion in a Li-ion cell, as well as optimization of practical energy conversion and storage processes using Li-ion cells.

Appendix A: Dimensional equations and non-dimensionalization scheme

Based on the assumptions listed in Sect. 2, the concentration conservation equations for separator and electrode layers may be written in dimensional form as follows:

$$\frac{\partial c_1}{\partial t} = D\frac{\partial^2 c_1}{\partial x^2} \tag{37}$$

and

$$\varepsilon\frac{\partial c_2}{\partial t} = D\varepsilon^{3/2}\frac{\partial^2 c_2}{\partial x^2} - \frac{I(t)\left(1-t_+\right)}{F\cdot L_2} \tag{38}$$

Note that the migration term is zero based on the common assumption of constant transference number [42]. The term $-\frac{I(t)\left(1-t_+\right)}{F\cdot L_c}$ appearing in Eq. (38) represents the pore wall flux, assumed to be uniform and constant [42]. The dimensional boundary conditions are

$$\frac{\partial c_1}{\partial x} = -\frac{I(t)\left(1-t_+\right)}{F\cdot D} \quad \text{at } x = 0 \tag{39}$$

$$c_1 = c_2 \quad \text{at } x = L_1 \tag{40}$$

$$\frac{\partial c_1}{\partial x} = \varepsilon^{3/2}\frac{\partial c_2}{\partial x} \quad \text{at } x = L_1 \tag{41}$$

$$\frac{\partial c_2}{\partial x} = 0 \quad \text{at } x = L_1 + L_2 \tag{42}$$

The initial condition is

$$c_1 = c_2 = c_0 \quad \text{at } t = 0 \tag{43}$$

The non-dimensional variables are defined as follows

$$\tau = \frac{Dt}{L_1^2};\quad \xi = \frac{x}{L_1};\quad C_1 = \frac{c_1}{c_0};\quad C_2 = \frac{c_2}{c_0} \tag{44}$$

Substituting in Eqs. (37)–(38), one may obtain the following non-dimensional governing equations:

$$\frac{\partial C_1}{\partial \tau} = \frac{\partial^2 C_1}{\partial \xi^2} \tag{45}$$

$$\frac{\partial C_2}{\partial \tau} = \sqrt{\varepsilon}\frac{\partial^2 C_2}{\partial \xi^2} + J(\tau) \tag{46}$$

where

$$J(\tau) = -I(\tau)\frac{\left(1-t_+\right)L_1^2}{FDL_2c_0\varepsilon} \tag{47}$$

Similarly, substituting in the boundary conditions, given by Eqs. (39)–(42), one may obtain

$$\frac{\partial C_1}{\partial \xi} = \varepsilon r J \quad \text{at } \xi = 0 \tag{48}$$

$$C_1 = C_2 \quad \text{at } \xi = 1 \tag{49}$$

$$\frac{\partial C_1}{\partial \xi} = \varepsilon^{3/2}\frac{\partial C_2}{\partial \xi} \quad \text{at } \xi = 0 \tag{50}$$

$$\frac{\partial C_2}{\partial \xi} = 0 \quad \text{at } \xi = 1 + r \tag{51}$$

where $r = L_2/L_1$. The initial condition in non-dimensional form is

$$C_1 = C_2 = 1 \quad \text{at } \tau = 0 \tag{52}$$

Equations (45)–(52) constitute the set of non-dimensional equations solved in this work (Eqs. (1)–(4)).

Acknowledgements This material is based upon work supported by CAREER Award No. CBET-1554183 from the National Science Foundation. This research was also supported by the Key Project of Science of the Education Bureau of Henan Province (Grant No. 19B460005), Special Project of Basic Scientific Research Operating Expenses of Henan Polytechnic University (Grant No. NSFRF180427), and China Scholarship Council.

References

1. Goodenough JB, Park K-S (2013) J Am Chem Soc 135:1167–1176
2. Scrosati B, Garche J (2010) J Power Sources 195:2419–2430
3. Parhizi M, Ahmed M, Jain A (2017) J Power Sources 370:27–35
4. Pasquier AD, Plitz I, Menocal S, Amatucci G (2003) J Power Sources 115:171–178
5. Shah K et al (2017) J Electrochem Energy Convers Storage 14:020801
6. Gomadam PM, Weidner JW, Dougal RA, White RE (2002) J Power Sources 110:267–284
7. Xiong R, Cao J, Yu Q, He H, Sun F (2018) IEEE Access 6:1832–1843
8. Xiao M, Choe S-Y (2012) J Power Sources 218:357–367
9. Nejad S, Gladwin D, Stone D (2016) J Power Sources 316:183–196
10. Zhang J, Lee J (2011) J Power Sources 196:6007–6014
11. Jokar A, Rajabloo B, Désilets M, Lacroix M (2016) J Power Sources 327:44–55
12. Jardine AK, Lin D, Banjevic D (2006) Mech Syst Signal Process 20:1483–1510
13. He H, Xiong R, Fan J (2011) Energies 4:582–598
14. He H, Zhang X, Xiong R, Xu Y, Guo H (2012) Energy 39:310–318
15. Santhanagopalan S, Guo Q, Ramadass P, White RE (2006) J Power Sources 156:620–628
16. Subramanian VR, Diwakar VD, Tapriyal D (2005) J Electrochem Soc 152:1–8
17. Newman J, Tiedemann W (1975) AIChE J 21:25–41
18. Doyle M, Fuller TF, Newman J (1993) J Electrochem Soc 140:1526–1533
19. Ramadesigan V et al (2012) J Electrochem Soc 159:31–45
20. Botte GG, Subramanian VR, White RE (2000) Electrochim Acta 45:2595–2609
21. Zhang Q, White RE (2007) J Power Sources 165:880–886
22. Subramanian VR, Ritter JA, White RE (2001) J Electrochem Soc 148:444–449
23. Cai L, White RE (2009) J Electrochem Soc 156:A154–A161
24. Luo W, Lyu C, Wang L, Zhang L (2013) J Power Sources 241:295–310
25. Fuller TF, Doyle M, Newman J (1994) J Electrochem Soc 141:1–10
26. Subramanian VR, Tapriyal D, White RE (2004) Electrochem Solid-State Lett 7:A259–A263
27. Ramadesigan V, Boovaragavan V, Pirkle JC, Subramanian VR (2010) J Electrochem Soc 157:A854–A867
28. Subramanian VR, Boovaragavan V, Ramadesigan V, Arabandi M (2009) J Electrochem Soc 156:A260–A271
29. Northrop PWC, Ramadesigan V, De S, Subramanian VR (2011) J Electrochem Soc 158:A1461–A1477
30. Ning G, Popov BN (2004) J Electrochem Soc 151:A1584–A1591
31. Rahimian SK, Rayman S, White RE (2013) J Power Sources 224:180–194
32. Doyle M, Newman J (1997) J Appl Electrochem 27:846–856
33. Subramanian VR, White RE (2001) J Power Sources 96:385–395
34. Atlung S (1979) J Electrochem Soc 126:1311–1321
35. Ali SH, Hussin A, Arof A (2002) J Power Sources 112:435–442
36. Johan MR, Arof AK (2004) Ionics 10:405–414
37. Liu S (2006) Solid State Ionics 177:53–58
38. Johan MR, Arof AK (2007) J Power Sources 170:490–494
39. Parhizi M, Jain A (2020) J Electrochem Soc 167:120544
40. Guo M, White RE (2012) J Power Sources 198:322–328
41. Verma S, Khosla A, Arya S (2020) J Electrochem Soc 167:120527
42. Newman J, Thomas-Alyea KE (2004) Electrochemical systems. Wiley, Hoboken
43. Wu X, Shi J-Y, Lei H, Li Y-P, Okine L (2019) J Central South Univ 26:3175–3187

Publisher's Note Springer Nature remains neutral with regard to jurisdictional claims in published maps and institutional affiliations.